Recombination Rates of $In_xGa_{1-x}N/Al_yGa_{1-y}N/GaN$ Multiple Quantum Wells Emitting From 640 to 565 nm

Syed Ahmed Al Muyeed, Damir Borovac, Haotian Xue, Xiongliang Wei, Renbo Song, Nelson Tansu, *Fellow, IEEE*, and Jonathan J. Wierer, Jr., *Senior Member, IEEE*

***Abstract*— The recombination rates in an $In_{0.25}Ga_{0.75}N/Al_{0.48}Ga_{0.52}N/GaN$ multiple quantum well (MQW) structure are measured to identify the cause of low efficiencies in high In-content InGaN quantum wells. The MQWs emit from 640 to 565 nm and are grown using metal-organic chemical vapor deposition (MOCVD). The addition of AlGaN interlayers within the MQW provides strain balancing and suppresses defect formation in high In-content InGaN quantum wells. The rates are found by transforming the optically measured radiative efficiency, differential carrier lifetimes, and optical absorption. Both components of non-radiative recombination rates, Shockley-Read-Hall (SRH) and Auger recombination, are found to be similar to the values of blue-emitting InGaN MQWs. The low SRH recombination rate is attributed to the use of the AlGaN interlayer. The radiative recombination rate, however, is more than an order of magnitude lower compared to blue emitting (lower In-content) InGaN-based MQWs. While this large reduction in radiative rate can be attributed to differences in carrier overlap and transition energy, it may also include effects of variations in thickness and compositional inhomogeneities.**

***Index Terms*—*ABC* coefficients, aluminum gallium nitride (AlGaN), differential carrier lifetime, gallium nitride (GaN), indium gallium nitride (InGaN), interlayer (IL), light-emitting diode (LED), metal-organic chemical vapor deposition (MOCVD), micro-display, multiple quantum well (MQW).**

I. Introduction

InGaN based multiple quantum wells (MQWs) are used as the active region for the highest efficiency violet-blue light emitting diodes (LEDs) and laser diodes [1]. Combining these LEDs with phosphors creates white light, and are predominately used in solid-state lighting (SSL) [2]. Recently, there has been a lot of focus on emissive displays using micro-LEDs [3], [4]. The challenges for micro-LEDs are very different to SSL LEDs [5], [6]. These LEDs need to operate at low to moderate current densities and emit in the red, green, and blue in order to create efficient and large color gamut displays [7]. While it is possible to produce these wavelengths using $In_xGa_{1-x}N$ emitters, the efficiency drastically decreases with increasing In content ($x \geq 0.20$), commonly known as the "green-gap" problem [8].

Several reasons are given as the cause of green gap, which include high lattice mismatch and phase separation in high In content QWs [9], [10], carrier localization due to fluctuations in InGaN composition [11], [12], low growth temperatures [13], [14], and low electron-hole wavefunction overlap due to spontaneous and piezoelectric polarization induced electric fields [15]. However, it is still not clear which is the dominant effect. To understand the role of these effects, different recombination mechanisms in the QWs need to be studied. One of the possible techniques is optical differential carrier lifetime (DCL) used in conjunction with radiative efficiency and optical absorption [16]. These measurements yield the non-radiative Shockley-Read-Hall (SRH) recombination, radiative recombination, and non-radiative Auger recombination rates and their associated A, B, and C coefficients [17].

It has been shown that employing AlGaN interlayers (ILs) grown on top $In_xGa_{1-x}N$ QWs can remarkably improve efficiencies at green to red wavelengths [18]–[21]. The addition of the $Al_yGa_{1-y}N$ IL improves the efficiency at long wavelengths by shifting the growth of the MQW to favorable conditions. The AlGaN IL is grown at the low QW temperatures to control In-content in the QW, and both the IL and QW are annealed during the higher temperature GaN barrier growth to improve crystallinity. The IL also provides strain-compensation to prevent defector formation [19], [22]. Another well-known method to improve efficiency is to include an InGaN UL which has been reported to stop defect propagation into the active region [23], [24]. Even after these improvements the efficiencies in the green-red are much lower compared to violet-blue. Improvements will require a deeper understand of the recombination dynamics within the quantum wells.

In this study, InGaN/AlGaN/GaN MQWs emitting at 640-565 nm are grown to measure the radiative and non-radiative recombination rates and coefficients, and compare

Manuscript received May 6, 2021; revised July 11, 2021 and August 21, 2021; accepted August 30, 2021. Date of publication September 10, 2021; date of current version September 22, 2021. This work was supported in part by the U.S. National Science Foundation under Grant 1708227. *(Corresponding author: Syed Ahmed Al Muyeed.)*

Syed Ahmed Al Muyeed, Damir Borovac, Haotian Xue, Xiongliang Wei, Renbo Song, and Jonathan J. Wierer, Jr., are with the Department of Electrical and Computer Engineering, Lehigh University, Bethlehem, PA 18015 USA, and also with the Center for Photonics and Nanoelectronics, Lehigh University, Bethlehem, PA 18015 USA (e-mail: sya216@lehigh.edu; jwierer@lehigh.edu).

Nelson Tansu is with the School of Electrical and Electronic Engineering (EEE), The University of Adelaide, Adelaide, SA 5005, Australia, and also with the Institute for Photonics and Advanced Sensing (IPAS), The University of Adelaide, Adelaide, SA 5005, Australia (e-mail: nelson.tansu@adelaide.edu.au).

Color versions of one or more figures in this article are available at https://doi.org/10.1109/JQE.2021.3111402.

Digital Object Identifier 10.1109/JQE.2021.3111402

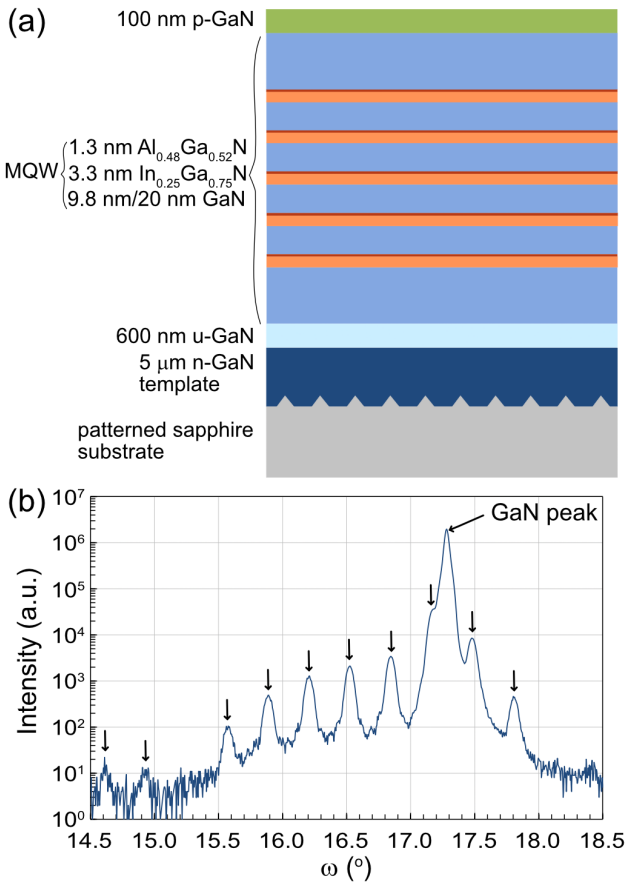

Fig. 1. (a) Shows a cross-sectional schematic of the 5-period multiple quantum well (MQW) structure grown on an n-GaN template. The layer thicknesses and compositions are determined by X-ray diffraction (XRD) and optical reflectance measurements. (b) Shows an XRD Omega-2theta scan of the sample along the (0002) reflection of GaN. The vertical arrows show the position of the MQW peaks.

to rates of MQWs emitting at shorter wavelengths. These recombination rates were yet to be measured at these long visible wavelengths. Radiative efficiency and differential carrier lifetimes are measured optically along with optical absorption. The data shows that the AlGaN IL provides control of SRH recombination. However, the radiative recombination rate is much lower compared to shorter wavelengths, showing that this is the area that needs to be improved to achieve higher efficiencies.

II. Experimental Details

The $In_xGa_{1-x}N/Al_yGa_{1-y}N/GaN$ MQW structure is repeated five times, and grown on a commercially available n-type doped (electron concentration of 5×10^{18} cm^{-3}) GaN template formed on c-plane patterned sapphire substrates using metal-organic chemical vapor deposition (MOCVD). A cross-sectional schematic is shown in Fig. 1(a). First, a 600 nm thick un-intentionally doped (uid) GaN layer is grown on the template at 1030 °C using trimethylgallium (TMGa) as the gallium precursor. Next, the first GaN quantum barrier and subsequent MQWs are grown using triethylgallium (TEGa), trimethylindium (TMIn), and trimethylaluminum (TMAl) as the group III precursors. The InGaN QWs and the AlGaN ILs are grown at 695 °C, whereas the barriers are grown at 905 °C. The high temperature growth of the GaN barriers is enabled by the AlGaN IL [22].

It has been shown that the n-type doping of the underlying layer can affect the position of the Fermi level in the active region, which affects the differential carrier lifetimes in the QWs [17]. Therefore, to make sure the Fermi level resides near mid-bandgap, a 100 nm p-type doped GaN layer is grown after the last barrier. This p-GaN layer is grown at a low temperature of 830 °C to protect the QWs, and at a high V-III ratio of 51,000. Hall measurement reveals that the hole concentration of this p-type GaN layer is 5×10^{16} /cm^3.

An X-ray diffraction (XRD) omega-2theta scan along (0002) reflection of GaN of the sample is shown in Fig. 1(b). This data is fitted to determine the thicknesses and compositions of the different layers in the active region. From these measurements, the In content in the QW is $x = 0.25$ and the Al content in the IL is $y = 0.48$. The QW, IL, and barrier thicknesses are 3.3 nm, 1.3 nm, and 9.8 nm, respectively. The first and the last GaN barriers are intentionally grown double the thickness at ~20 nm.

Photoluminescence (PL) is performed at both 8 K and room temperature with a 405 nm laser diode under continuous-wave operation and at power densities varying from ~1.5 W/cm^2 to ~7000 W/cm^2 to determine the peak wavelength and radiative efficiency (η_{rad}) versus the steady-state carrier density (N). This large pump power density range is achieved by varying the laser power from ~5 mW to ~370 mW; and varying the laser beam diameter from ~470 μm to ~82 μm. Light spectra are measured using a high-resolution spectrometer. The method to determine the absolute η_{rad} is detailed in [21]. The radiative efficiency is defined as:

$$\eta_{rad} = R_R/(R_R + R_{NR}), \tag{1}$$

where R_R is the radiative recombination rate and R_{NR} is the non-radiative recombination rate. Optical absorption of the sample at 405 nm is measured by performing white light reflectance and transmission with an integrating sphere. The absorption of the MQWs is 19%.

The differential carrier lifetimes, τ_{DCL} are obtained by an all-optical measurement using the methods similar to previous reports [16], [21]. The MQW samples are again excited with a 405 nm laser diode that is driven by combining (with a bias tee) a constant bias (constant carrier density) and small-signal sinusoidal bias frequencies, f, between 0.05 and 500 MHz provided by a vector network analyzer (VNA). The constant bias of the laser diode is changed to measure τ_{DCL} at different power densities, thus different carrier densities. The differential carrier lifetimes, τ_{DCL} at different power densities is determined from phase and amplitude differences of the input (laser) and output (MQW) signals, using the small-signal response F, expressed as [25]:

$$F = 1/\left(1 + j2\pi\,\tau_{DCL}\right). \tag{2}$$

The radiative (R_R) and non-radiative (R_{NR}) recombination rates versus N are obtained by transforming the measured data

the following way. The generation rate is defined by

$$G = P/(h\upsilon/q)\,, \tag{3}$$

where P is the absorbed power density of the pump laser. The carrier density is found integrating τ_{DCL} with respect to G, expressed as

$$N = \int_0^G \tau_{DCL} dG. \tag{4}$$

Finally, the radiative and nonradiative rates are found using

$$\frac{dR_R}{dN} = \eta_{rad}\tau_{DCL}^{-1} + G\frac{d\eta_{rad}}{dn}, \tag{5a}$$

$$\frac{dR_{NR}}{dn} = (1-\eta_{rad})\,\tau_{DCL}^{-1} - \mathrm{G}\frac{d\eta_{rad}}{dn}. \tag{5b}$$

Integrating Eqns. 5a and 5b give the radiative and non-radiative rates versus the carrier density found in Equation 4.

These rates are dynamic, varying with carrier density. Instead of rates, the recombination physics are commonly distilled down to *A, B,* and *C* coefficients (constant values). While the dynamic rates preclude constant coefficients, they are used here to compare to previous results. From these rates, the SRH recombination coefficient *A*, radiative recombination coefficient, *B* and Auger defect recombination coefficient, *C* are determined [26] by

$$A = \frac{R_{NR}}{N}, \quad B = \frac{R_R}{N^2}, \; C = \frac{(R_{NR} - AN)}{N^3}. \tag{6}$$

The equation for the A coefficient is only valid for low carrier densities ($N < 10^{17}/\ \mathrm{cm}^3$) where SRH recombination dominates the non-radiative rate, and the equation for C is valid only at high carrier densities ($N > 10^{19}/\ \mathrm{cm}^3$) where Auger recombination dominates the non-radiative rate.

III. Results and Discussion

Fig. 2(a) shows the spectra measured at pump power densities of ~57 W/cm^2 to ~7000 W/cm^2. These spectra are measured by collecting the light through a 450 nm long-pass filter to avoid the laser tail. Fig. 2(b) shows the change in peak wavelength and the full width at half-maximum (FWHM) with respect to the pump power density. At low power density of ~1.5 W/cm^2, the sample emits at 640 nm. As *N* increases with pump power density, carrier screening and phase-space filling is observed causing a gradual blueshift [27], [28], with the sample emitting at 565 nm at ~7000 W/cm^2. At the peak η_{rad} value the sample emits at 583 nm. The FWHM behavior is a bit more complex. At low power densities there is a narrowing of the FWHM, and the smallest FWHM is ~57 nm, occurring between ~25 W/cm^2 to ~200 W/cm^2. This FWHM is similar to the best reported at these longer wavelengths for InGaN [29]–[31]. At the highest power densities there is a gradual increase in the FWHM owing to band-filling and heating due to increased non-radiative Auger recombination.

Fig. 3(a) shows the radiative efficiency, η_{rad}, versus the laser input power density at room temperature. The peak radiative efficiency for this sample is ~3.85% at a power density of ~2 kW/cm^2. The η_{rad} measured at 224 W/cm^2 is 2.95% at 604 nm. Absorption, DCL measurement along with η_{rad}

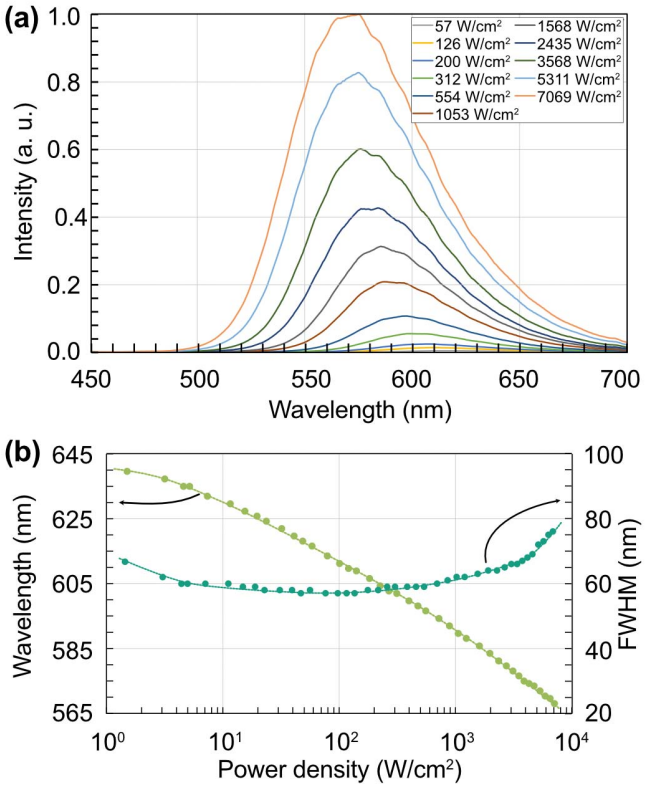

Fig. 2. (a) Shows the spectra measured at pump power densities of ~57 W/cm^2 to ~7000 W/cm^2. (b) Shows plot of peak wavelength and fullwidth at half-maximum (FWHM) versus the exciting power density. The peak wavelength shows a gradual blueshift with increasing power density and ranges from 640 nm to 568 nm. The FWHM has a minima of 57 nm and shows a gradual increase with power density.

determine the carrier density as $N = 3 \times 10^{18}$ cm^{-3} at this power density. This radiative efficiency could be further improved by tuning the IL thickness and Al composition [19], [21] and growing an In-containing UL before the QW [32], [33]. However, using this active region in a state-of-the-art thin-film LED with ~80% extraction efficiency would result in a peak external quantum efficiency of 2.3% at 604 nm which is comparable to others [29]. Fig. 3(b) shows the differential carrier lifetime, τ_{DCL}, of the sample with respect to pump power density. The τ_{DCL} values are longest at the lowest power densities. This is expected as at these values only SRH defect recombination is significant. As the power density increases the other recombination mechanisms, i.e., radiative and Auger recombination, start becoming significant and the τ_{DCL} values decrease.

The result of the transformation of the measured data in Fig. 3 to the recombination rates is shown in Fig. 4. Contrary to the traditional *ABC* model, the radiative and non-radiative recombination rates show carrier density dependance. Therefore, a better model needs to be developed to properly understand the complex recombination process inside the MQW. However, in this study the *A*, *B* and *C* coefficients are determined at specific carrier densities to compare with previously published reports.

Fig. 4(a) shows the R_{NR}/N versus *N*. Non-radiative recombination is caused by SRH and Auger recombination. The SRH

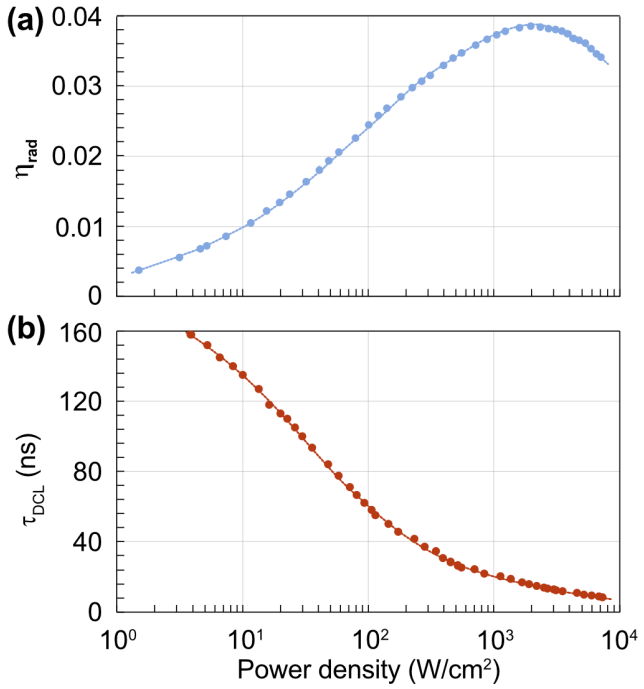

Fig. 3. Plots of (a) the radiative efficiency, η_{rad} and (b) optically measured differential carrier lifetime, τ_{DCL} versus the power density of the exciting laser at room temperature. The peak radiative efficiency is 3.85% occurring at 2 kW/cm^2. The τ_{DCL} ranges from 1.58 $\times$ 10^{-7} s to 8.5 $\times$ 10^{-9} s across the input power density range.

recombination is a mono-molecular process and is dominant at low carrier densities. Therefore, R_{NR}/N versus N is constant at low carrier densities and yields the value of the A coefficient. It is 5.73 $\times$ 10^6 s^{-1} at $N = 6 \times 10^{16}$ cm^{-3}. This low A coefficient value is achieved due to the AlGaN IL which allows the growth of the barriers at a much higher temperature compared to conventional InGaN/GaN MQWs and helps with the radiative efficiency of the InGaN [22]. This can potentially be further improved by tuning the growth conditions and growing an InGaN UL before the MQW [17], [32].

This A coefficient value is comparable to the values previously reported for InGaN-based MQWs at shorter wavelengths when the MQW is grown without an In containing UL [21], [26], [34], [35]. Table I shows the A coefficient comparison at different wavelengths.

Fig. 4 (b) shows the R_R/N^2 versus N. Radiative recombination rate is a bi-molecular process, and the value of R_R/N^2 yields the value of the B coefficient. Fig 4(b) shows that B is not a constant, but rather it varies with N. This is similar to reports at shorter wavelengths [17]. At low N, B increases due to attractive Coulomb interaction between electrons and holes [36], [37]. Then as carrier density increases, this effect is screened and the R_R/N^2 gradually becomes constant. As the carrier density is further increased ($N \geq 5 \times 10^{18}$ cm^{-3}) the electron-hole wavefunction overlap increases due to carrier screening of piezoelectric polarization induced electric field [38] causing a slight increase in R_R/N^2. Finally, at the highest carrier densities, phase-space filling dominates and causes $R_R \propto N^a$ where $a < 2$ and a decrease in the R_R/N^2 is observed [34], [39].

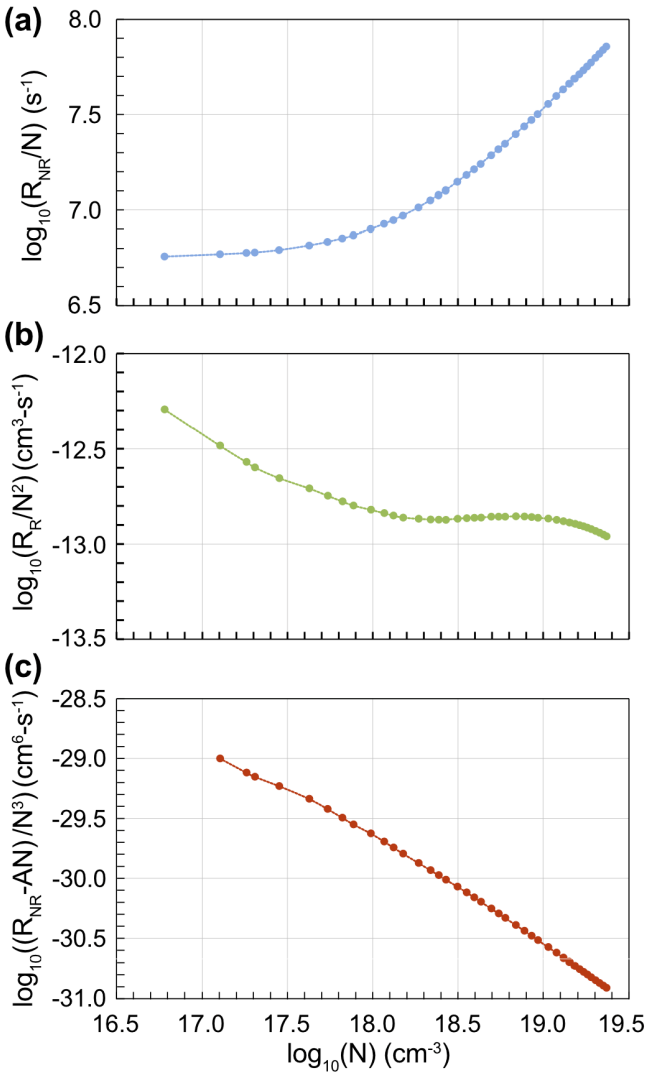

Fig. 4. Plots of the (a) nonradiative recombination rate (R_{NR}) divided by steady-state carrier density (N), (b) radiative recombination rate (R_R) divided by N^2, and (c) $(R_{NR} - AN)/N^3$ versus N. R_{NR}/N is constant at $N < 10^{17}$ cm^{-3} and corresponds to the SRH non-radiative coefficient A, which is 5.73 $\times$ 10^6 s^{-1}. R_R/N^2 yields the radiative recombination coefficient B. B at $N = 3 \times 10^{18}$ cm^{-3} is 1.4 $\times$ 10^{-13} cm^{3}s^{-1}. $(R_{NR} - AN)/N^3$ yields the Auger recombination coefficient C at high N ($>10^{19}$ cm^{-3}). At $N = 2.3 \times 10^{19}$ cm^{-3}, $C = 1.25 \times 10^{-31}$ cm^{6}s^{-1}.

Table I also shows the B coefficients for the present sample at $N = 3 \times 10^{18}$ cm^{-3}, typical LED operating carrier density, $B = 1.4 \times 10^{-13}$ cm^{3}s^{-1} and values provided in the literature for blue and green. The measured B coefficient is ~16 times lower than the values in the blue (470 nm) and falls in trend with the previously published results that show gradual reduction in B with decreasing transition energy [21], [34], [40]. It should be noted that the data from [34] and [35] in Table I do not have an IL. One would expect the addition of the IL will increase the polarization fields on the quantum well and decrease the electron hole overlap. However, this is counteracted by an increase in the barrier from the IL. The decrease in the overlap calculated by Schrodinger-Poisson k.p simulations is small (<1%) [21], and therefore, we are able to reasonably compare MQWs with and without ILs.

TABLE I
COMPARISON OF *A* AND *B* COEFFICIENTS AT DIFFERENT WAVELENGTHS

Study	Peak Wavelength (nm)	*A* coefficient ($x10^6$ s^{-1})	*B* coefficient ($x10^{-13}$ cm^3s^{-1})
Ref. [34]	470	4	22
Ref. [35]	522	4.7	12
Ref. [21]	573	3-6	2-4
This study	604	5.73	1.4

There are few reasons behind this reduction in B. The B coefficient can be expressed as:

$$B \propto E_{eh} \left|\hat{e} \cdot p_{eh}\right|^2 |I|^2 \mathcal{L}(E_{eh}). \quad (7)$$

From Eqn. (7), the three terms on the right-hand side will decrease with increased In-content in the QWs [41], [42]. They are the transition energies, E_{eh}, electron-hole overlap, $|I|^2$, and momentum matrix element squared, ($\left|\hat{e} \cdot p_{eh}\right|^2$). At $N = 3 \times 10^{18}$ cm^{-3}, the electron-hole wavefunction overlap, I, of the present structure is ~9-10 %. Compared to a blue-emitting MQW (with 3.3 nm thick $In_{0.15}Ga_{0.85}N$ QWs and 10 nm thick GaN barriers), there is an $|I|^2$ ratio reduction of ~3.6 times. The ratios of $\left|\hat{e} \cdot p_{eh}\right|^2$ and E_{eh} contribute to reductions of ~2 times [43] and ~1.3 times, respectively. The combined contributions of all these elements attribute to ~9.4 times reduction in B coefficient, smaller than the experimental trend.

Other likely effects causing the additional decrease are compositional and thickness variations in the quantum wells which are manifest in the broadening term ($\mathcal{L}(E_{eh})$) in the B coefficient. Recent reports have suggested that carrier localization due to compositional variations affect B by changing the momentum-matrix element and the linewidth [11], [44], [45]. Thickness variation in InGaN QWs is another reason that could potentially decrease B [46]. Further studies need to be conducted to understand the full effect of all these non-idealities, but clearly improvements in the B coefficient will lead to higher efficiencies.

Finally, Fig. 4 (c) shows the $(R_{NR} - AN)/N^3$ versus N, where the A coefficient is determined at low carrier densities. $(R_{NR} - AN)$ is the Auger recombination rate portion of the total non-radiative recombination rate which dominates at the high carrier densities ($N \geq 1 \times 10^{19}$ cm^{-3}). The Auger recombination coefficient, C is 1.25×10^{-31} cm^6s^{-1} at $N = 2.3 \times 10^{19}$ cm^{-3}. This value is once again similar to the value in blue when grown without an UL [26]. Auger recombination has two components: interband Auger recombination and defect assisted Auger recombination [26]. Additionally, Auger recombination is also affected by both carrier screening and phase-space filling. To get a full grasp of C, samples of different defect densities need be measured at higher N.

Previous reports suggest that all three A, B, and C coefficients are related to overlap and should decrease at longer wavelengths [34]. In an ideal case, where the defect density remains similar, the effect of wavefunction overlap change should get cancelled and the η_{rad} should vary by a small amount. However, the trend versus wavelength (or In content in the QW) observed here is different. The B coefficient decreases with an increase in wavelength, as expected, but its decrease is more rapid than simply due to the overlap as discussed. The A and C should decrease as the overlap to approximately the power of 1 and 3, respectively [17], [26], [47], but experimentally they are comparable to lower In-content QWs. This has implications on the radiative efficiency that can be expressed as $\eta_{rad} = BN^2/(AN + BN^2)$ if we ignore C for now. This more rapid decrease in B/A ratio versus wavelength (Table I) is the main reason behind lower efficiencies at longer wavelengths for InGaN-based LEDs. Employing an AlGaN IL has provided some control of the A coefficient and C coefficients compared to a conventional orange-yellow InGaN/GaN MQW, but in theory they should be even smaller. Therefore, if A can be lowered by further reducing the defect density and fixing the inhomogeneities that also lower B, then it will lead to a larger improvements in efficiency.

Finally, it should be noted that the addition of an IL may affect the eventual carrier distribution in the MQWs and resistance while under electrical injection. It is known that in conventional MQWs without an IL that lower hole mobilities limits uniform injection across the QWs, so that deeper QWs (further from p-type layers), have less carriers. The addition of an IL may exasperate this problem. Electrically injected LEDs with IL-MQWs have shown impressive results [29], [48], with impressive resistances and forward bias characteristics. The ILs are thin and have large energy band tilts that could help with tunneling. It is unclear what the exact carrier spreading is in these structures. Spreading is of great concern because injecting into less QWs will increase carrier densities at a particular current, inducing Auger recombination at lower currents. The benefit of the optical pump methods used in this work are that they remove these additional considerations, making for a simpler rate analysis. For electrically injected structures, additional analysis will be required to determine if the increase in radiative efficiency is counteracted by any additional resistances or carrier injection issues.

IV. CONCLUSION

To conclude, an InGaN/AlGaN/GaN MQW structure emitting from 640 nm to 565 nm is grown specifically for optical determination of the radiative and non-radiative recombination coefficients. The measured data reveals that growing an AlGaN IL on top of the InGaN QW results in a SRH recombination rate similar to MQWs emitting at shorter wavelengths. Yet, the radiative efficiency is much lower compared to shorter wavelengths due to a ~16 times reduction in the B coefficient. Additionally, the A coefficient should be lower based on its dependance on overlap. The B/A ratio is decreasing more than predicted by a simple overlap argument. Therefore, methods that lead to further defect reductions and other non-ideal effects causing should be further studied.

REFERENCES

[1] J. Y. Tsao *et al.*, "Toward smart and ultra-efficient solid-state lighting," *Adv. Opt. Mater.*, vol. 2, no. 9, pp. 809–836, 2014.

[2] Y. Narukawa, M. Ichikawa, D. Sanga, M. Sano, and T. Mukai, "White light emitting diodes with super-high luminous efficacy," *J. Phys. D, Appl. Phys.*, vol. 43, no. 35, 2010, 354002.

[3] K. Sakariya, A. Bibl, and H. Hu, "Active matrix emissive micro led display," U.S. 9343448 B2, May 17, 2016.

[4] J. Day, J. Li, D. Y. C. Lie, C. Bradford, J. Y. Lin, and H. X. Jiang, "III-Nitride full-scale high-resolution microdisplays," *Appl. Phys. Lett.*, vol. 99, no. 3, 2011, Art. no. 031116.

[5] F. Olivier, S. Tirano, L. Dupré, B. Aventurier, C. Largeron, and F. Templier, "Influence of size-reduction on the performances of GaN-based micro-LEDs for display application," *J. Lumin.*, vol. 191, pp. 112–116, Nov. 2017.

[6] K. Bulashevich, S. Konoplev, and S. Karpov, "Effect of die shape and size on performance of III-nitride micro-LEDs: A modeling study," *Photonics*, vol. 5, no. 4, p. 41, Oct. 2018.

[7] J. J. Wierer and N. Tansu, "III-nitride Micro-LEDs for efficient emissive displays," *Laser Photon. Rev.*, vol. 13, no. 9, Sep. 2019, Art. no. 1900141.

[8] M. R. Krames *et al.*, "Status and future of high-power light-emitting diodes for solid-state lighting," *J. Display Technol.*, vol. 3, no. 2, pp. 160–175, Jun. 2007.

[9] D. D. Koleske, S. R. Lee, M. H. Crawford, K. C. Cross, M. E. Coltrin, and J. M. Kempisty, "Connection between GaN and InGaN growth mechanisms and surface morphology," *J. Cryst. Growth*, vol. 391, pp. 85–96, Apr. 2014.

[10] N. A. El-Masry, E. L. Piner, S. X. Liu, and S. M. Bedair, "Phase separation in InGaN grown by metalorganic chemical vapor deposition," *Appl. Phys. Lett.*, vol. 72, p. 40, Jan. 1998.

[11] M. A. D. Maur, A. Pecchia, G. Penazzi, W. Rodrigues, and A. D. Carlo, "Efficiency drop in green InGaN/GaN light emitting diodes: The role of random alloy fluctuations," *Phys. Rev. Lett.*, vol. 116, no. 2, 2016, Art. no. 027401.

[12] S. Karpov, "Effect of carrier localization on recombination processes and efficiency of InGaN-based LEDs operating in the 'green gap,'" *Appl. Sci.*, vol. 8, no. 5, p. 818, May 2018.

[13] D. D. Koleske, A. E. Wickenden, R. L. Henry, and M. E. Twigg, "Influence of MOVPE growth conditions on carbon and silicon concentrations in GaN," *J. Cryst. Growth*, vol. 242, nos. 1–2, pp. 55–69, 2002.

[14] A. M. Armstrong, M. H. Crawford, and D. D. Koleske, "Contribution of deep-level defects to decreasing radiative efficiency of InGaN/GaN quantum wells with increasing emission wavelength," *Appl. Phys. Exp.*, vol. 7, no. 3, Mar. 2014, Art. no. 032101.

[15] U. T. Schwarz, H. Braun, K. Kojima, Y. Kawakami, S. Nagahama, and T. Mukai, "Interplay of built-in potential and piezoelectric field on carrier recombination in green light emitting InGaN quantum wells," *Appl. Phys. Lett.*, vol. 91, no. 12, Sep. 2007, Art. no. 123503.

[16] A. David, N. G. Young, C. A. Hurni, and M. D. Craven, "All-optical measurements of carrier dynamics in bulk-GaN LEDs: Beyond the ABC approximation," *Appl. Phys. Lett.*, vol. 110, no. 25, Jun. 2017, Art. no. 253504.

[17] A. David, N. G. Young, C. Lund, and M. D. Craven, "Review—The physics of recombinations in III-nitride emitters," *ECS J. Solid State Sci. Technol.*, vol. 9, no. 1, Jan. 2020, Art. no. 016021.

[18] S. Saito, R. Hashimoto, J. Hwang, and S. Nunoue, "InGaN light-emitting diodes on *c*-face sapphire substrates in green gap spectral range," *Appl. Phys. Exp.*, vol. 6, no. 11, Nov. 2013, Art. no. 111004.

[19] S. A. A. Muyeed *et al.*, "Strain compensation in InGaN-based multiple quantum wells using AlGaN interlayers," *AIP Adv.*, vol. 7, no. 10, Oct. 2017, Art. no. 105312.

[20] W. Sun, S. A. Al Muyeed, R. Song, J. J. Wierer, Jr., and N. Tansu, "Integrating AlInN interlayers into InGaN/GaN multiple quantum wells for enhanced green emission," *Appl. Phys. Lett.*, vol. 112, no. 20, 2018, Art. no. 201106.

[21] S. A. Al Muyeed *et al.*, "Recombination rates in green-yellow InGaN-based multiple quantum wells with AlGaN interlayers," *J. Appl. Phys.*, vol. 126, no. 21, Dec. 2019, Art. no. 213106.

[22] D. D. Koleske, A. J. Fischer, B. N. Bryant, P. G. Kotula, and J. J. Wierer, "On the increased efficiency in InGaN-based multiple quantum wells emitting at 530–590 nm with AlGaN interlayers," *J. Cryst. Growth*, vol. 415, pp. 57–64, Apr. 2015.

[23] A. M. Armstrong, B. N. Bryant, M. H. Crawford, D. D. Koleske, S. R. Lee, and J. J. Wierer, Jr., "Defect-reduction mechanism for improving radiative efficiency in InGaN/GaN light-emitting diodes using InGaN underlayers," *J. Appl. Phys.*, vol. 117, no. 13, Apr. 2015, Art. no. 134501.

[24] C. Haller, J.-F. Carlin, M. Mosca, M. D. Rossell, R. Erni, and N. Grandjean, "InAlN underlayer for near ultraviolet InGaN based light emitting diodes," *Appl. Phys. Exp.*, vol. 12, no. 3, Feb. 2019, Art. no. 034002.

[25] I. Reklaitis *et al.*, "Differential carrier lifetime in InGaN-based light-emitting diodes obtained by small-signal frequency-domain measurements," *J. Appl. Phys.*, vol. 121, no. 3, Jan. 2017, Art. no. 035701.

[26] A. David, N. G. Young, C. A. Hurni, and M. D. Craven, "Quantum efficiency of III-nitride emitters: Evidence for defect-assisted nonradiative recombination and its effect on the green gap," *Phys. Rev. A, Gen. Phys.*, vol. 11, no. 3, Mar. 2019, Art. no. 031001.

[27] J. Zhang and N. Tansu, "Improvement in spontaneous emission rates for InGaN quantum wells on ternary InGaN substrate for light-emitting diodes," *J. Appl. Phys.*, vol. 110, no. 11, Dec. 2011, Art. no. 113110.

[28] S. J. Chang, W. C. Lai, Y. K. Su, J. F. Chen, C. H. Liu, and U. H. Liaw, "InGaN-GaN multiquantum-well blue and green light-emitting diodes," *IEEE J. Sel. Topics Quantum Electron.*, vol. 8, no. 2, pp. 278–283, Apr. 2002.

[29] J.-I. Hwang, R. Hashimoto, S. Saito, and S. Nunoue, "Development of InGaN-based red LED grown on (0001) polar surface," *Appl. Phys. Exp.*, vol. 7, no. 7, Jul. 2014, Art. no. 071003.

[30] Y. Robin, M. Pristovsek, H. Amano, F. Oehler, R. A. Oliver, and C. J. Humphreys, "What is red? On the chromaticity of orange-red InGaN/GaN based LEDs," *J. Appl. Phys.*, vol. 124, no. 18, Nov. 2018, Art. no. 183102.

[31] Z. Zhuang, D. Iida, and K. Ohkawa, "Investigation of InGaN-based red/green micro-light-emitting diodes," *Opt. Lett.*, vol. 46, no. 8, pp. 1912–1915, 2021.

[32] Y. Chen, C. Haller, W. Liu, S. Y. Karpov, J.-F. Carlin, and N. Grandjean, "GaN buffer growth temperature and efficiency of InGaN/GaN quantum wells: The critical role of nitrogen vacancies at the GaN surface," *Appl. Phys. Lett.*, vol. 118, no. 11, Mar. 2021, Art. no. 111102.

[33] F. Jiang *et al.*, "Efficient InGaN-based yellow-light-emitting diodes," *Photon. Res.*, vol. 7, no. 2, p. 144, 2019.

[34] A. David and M. J. Grundmann, "Influence of polarization fields on carrier lifetime and recombination rates in InGaN-based light-emitting diodes," *Appl. Phys. Lett.*, vol. 97, no. 3, Jul. 2010, Art. no. 033501.

[35] A. Laubsch, M. Sabathil, J. Baur, M. Peter, and B. Hahn, "High-power and high-efficiency," *IEEE Trans. Electron Devices*, vol. 57, no. 1, pp. 79–87, Dec. 2010.

[36] S. W. Koch, M. Kira, G. Khitrova, and H. M. Gibbs, "Semiconductor excitons in new light," *Nature Mater.*, vol. 5, no. 7, pp. 523–531, Jul. 2006.

[37] S. Chatterjee *et al.*, "Excitonic photoluminescence in semiconductor quantum wells: Plasma versus excitons," *Phys. Rev. Lett.*, vol. 92, no. 6, Feb. 2004, Art. no. 067402.

[38] W. Chow, M. Kira, and S. W. Koch, "Microscopic theory of optical nonlinearities and spontaneous emission lifetime in group-III nitride quantum wells," *Phys. Rev. B, Condens. Matter*, vol. 60, no. 3, pp. 1947–1952, Jul. 1999.

[39] J. Hader, J. V. Moloney, and S. W. Koch, "Beyond the ABC: Carrier recombination in semiconductor lasers," in *Proc. Int. Conf. Numer. Simul. Semiconductor Optoelectronic Devices*, vol. 6115, Feb. 2006, Art. no. 61151T.

[40] D. Schiavon, M. Binder, M. Peter, B. Galler, P. Drechsel, and F. Scholz, "Wavelength-dependent determination of the recombination rate coefficients in single-quantum-well GaInN/GaN light emitting diodes," *Phys. Status Solidi B*, vol. 250, no. 2, pp. 283–290, 2013.

[41] H. Zhao, G. Liu, J. Zhang, J. D. Poplawsky, V. Dierolf, and N. Tansu, "Approaches for high internal quantum efficiency green InGaN light-emitting diodes with large overlap quantum wells," *Opt. Exp.*, vol. 19, no. S4, pp. A991–A1007, 2011.

[42] R. A. Arif, Y. K. Ee, and N. Tansu, "Polarization engineering via staggered InGaN quantum wells for radiative efficiency enhancement of light emitting diodes," *Appl. Phys. Lett.*, vol. 91, no. 9, pp. 1–4, 2007.

[43] H. Zhao, R. A. Arif, and N. Tansu, "Self-consistent gain analysis of type-II 'W' InGaN–GaNAs quantum well lasers," *J. Appl. Phys.*, vol. 104, no. 4, Aug. 2008, Art. no. 043104.

[44] C. M. Jones, C.-H. Teng, Q. Yan, P.-C. Ku, and E. Kioupakis, "Impact of carrier localization on recombination in InGaN quantum wells and the efficiency of nitride light-emitting diodes: Insights from theory and numerical simulations," *Appl. Phys. Lett.*, vol. 111, no. 11, Sep. 2017, Art. no. 113501.

[45] D. S. P. Tanner, P. Dawson, M. J. Kappers, R. A. Oliver, and S. Schulz, "Polar (In,Ga)N/GaN quantum wells: Revisiting the impact of carrier localization on the 'green gap' problem," *Phys. Rev. A, Gen. Phys.*, vol. 13, no. 4, Apr. 2020, Art. no. 044068.
[46] G. H. Gu, D. H. Jang, K. B. Nam, and C. G. Park, "Composition fluctuation of in and well-width fluctuation in InGaN/GaN multiple quantum wells in light-emitting diode devices," *Microsc. Microanalysis*, vol. 19, no. S5, pp. 99–104, Aug. 2013.
[47] A. David, C. A. Hurni, N. G. Young, and M. D. Craven, "Field-assisted Shockley-Read-Hall recombinations in III-nitride quantum wells," *Appl. Phys. Lett.*, vol. 111, no. 23, Dec. 2017, Art. no. 233501.
[48] A. I. Alhassan *et al.*, "High luminous efficacy green light-emitting diodes with AlGaN cap layer," *Opt. Exp.*, vol. 24, no. 16, pp. 17868–17873, 2016.

Syed Ahmed Al Muyeed received the B.S. and M.S. degrees from the Department of Electrical and Electronic Engineering, University of Dhaka, Bangladesh, in 2014 and 2016, respectively, and the Ph.D. degree in electrical engineering from Lehigh University, in May 2021. He is currently a member of the Technical Staff at Raxium, Inc., Fremont, CA, USA. His research interests include the physics, growth, and characterization of III-Nitride semiconductor light emitters, especially in the visible range.

Damir Borovac received the B.S. and Ph.D. degrees in electrical engineering from Lehigh University, in 2015 and 2020, respectively. He is currently working as a Hardware Development Engineer at Osram Opto Semiconductors GmbH, Regensburg, Germany. He has coauthored over 60 publications and conference publications. His research interests include III-nitride material science and device physics.

Haotian Xue received the B.S. degree in applied physics from the University of Science and Technology of China and the M.S. degree in electrical engineering from Lehigh University, in 2020, where he is currently pursuing the Ph.D. degree, researching growth of III-Nitride semiconductors for power devices and light emitters.

Xiongliang Wei received the B.S. degree in optical information science and technology from Wuhan University, China, in 2014, and the M.S. degree in photonics and the Ph.D. degree in electrical engineering from Lehigh University, in 2016 and August 2021, respectively. His research focuses on simulation and fabrication of III-Nitride semiconductor quantum dot active layers to produce the next generation of high-efficiency light-emitting diodes and laser diodes.

Renbo Song received the B.S. and M.S. degrees in optics and condensed matter physics from Shandong University, China, in 1998 and 2001, respectively, and the Ph.D. degree in electrical engineering from Lehigh University, Bethlehem, PA, USA, in 2009. He worked as a MOCVD Scientist for Valence Process Equipment, from 2011 to 2015, and since then as the Scientific Manager with Lehigh University. His areas of interests include MOCVD and new epitaxy technologies for wide bandgap semiconductors.

Nelson Tansu (Fellow, IEEE) has been the Head of the School of Electrical and Electronics Engineering and a Professor of quantum electronics at The University of Adelaide, Adelaide, SA, Australia, since January 2021. Previously, he was the Daniel E. '39 and Patricia M. Smith Endowed Chair Professor with the Department of Electrical and Computer Engineering (ECE) and the Director of the Center for Photonics and Nanoelectronics (CPN) at Lehigh University. He had made advances to the invention and innovation, fundamental sciences, and device technologies of III-V and III-Nitride semiconductors. He holds more than 18 U.S. patents, and his work is integrated into today's state-of-the-art solid-state lighting technology. He has authored more than 160 refereed journals and 325 conference publications. He is currently a fellow of the U.S. National Academy of Inventors (NAI Fellow; elected in 2016) and Clarivate Analytics Highly Cited Researcher in 2018. He is the Editor-in-Chief of the open-access journal *Photonics*, and he serves as a member of the editorial boards for eight other leading journals in applied physics and nanotechnology.

Jonathan J. Wierer, Jr. (Senior Member, IEEE) received the B.S., M.S., and Ph.D. degrees in electrical engineering from the University of Illinois, Urbana–Champaign, IL, USA, in 1994, 1995, and 1999, respectively. He is currently a Professor with the Department of Electrical and Computer Engineering, North Carolina State University, Raleigh, NC, USA. Previously, he was with Philips-Lumileds, San Jose, CA, USA; Sandia National Laboratories, Albuquerque, NM, USA; and Lehigh University, Bethlehem, PA, USA. His research highlights include developing the first high-power (1 Watt) flip-chip III-nitride LED and proposing laser diodes as an ultra-efficient light source for solid-state lighting. He has authored or coauthored over 180 publications and conference publications and holds 42 patents, predominately related to III-nitride devices.